Thermo-mechanical simulation of track development in the Laser Beam Melting process - Effect of laser-metal interaction

IOP Conf. Series: Materials Science and Engineering **529** (2019) 012005 doi:10.1088/1757-899X/529/1/012005

Thermo-mechanical simulation of track development in the Laser Beam Melting process - Effect of laser-metal interaction

Alexis Queva[1,3], Yaasin Mayi[2,3], Michel Bellet[1], Gildas Guillemot[1], Patrice Peyre[2], Morgan Dal[2], Clara Moriconi[3], Charlotte Metton[3]

[1] *MINES ParisTech, PSL Research University, CEMEF – Centre de mise en forme des matériaux, CNRS UMR 7635, CS 10207 rue Clause Daunesse, 06904 Sophia Antipolis Cedex, France*
[2] *PIMM Laboratory, UMR 8006 CNRS – Arts et Métiers ParisTech, 151 Bd de l'Hôpital, 75013 Paris, France*
[3] *Safran, site de Paris-Saclay, Rue des Jeunes Bois - Chateaufort, CS 80112 78772 Magny-les Hameaux*

Production Editor, *Journal of Physics: Conference Series*, IOP Publishing, Dirac House, Temple Back, Bristol BS1 6BE, UK

E-mail: alexis.queva@mines-paristech.fr

Résumé. Interest has recently emerged for the manufacture of aeronautical parts by Laser Beam Melting (LBM) additive process. This energy efficient process can for instance be used to build complex geometries, which cannot be made with traditional processes. However, complex phenomena occur during powder melting and track development : vaporisation phenomena influence laser-matter interaction by creating metal vapours that are responsible for the reduction of absorbed energy. The recoil pressure generated by the vaporisation counteracts the surface tension between the melt pool and the inert gas, also inducing liquid instabilities. The study of laser-matter interaction and induced phenomena can help understand the origin of defects such as porosities or cracks. In this approach, a level-set modelling of the LBM process at a mesoscopic scale is proposed to follow melt pool evolution and track development during build. A volume heat source model is used for laser/powder interaction considering the material absorption coefficient. A surface heat source is used to take into account the high laser energy absorption by dense metal alloys. An energy solver is coupled with thermodynamic database and pre-determined solidification path. Shrinkage during consolidation from powder to liquid and compact medium is modelled by a compressible Newtonian constitutive law. An automatic remeshing adaptation is also used to save time and avoid high computational cost. In the future, the computation of multiple beads or the build of a wall in a context of lattice structures will have to be considered.

1. Introduction

The LBM process is attractive for aeronautical applications. More specifically, manufacturing of complex shapes or one-pieces with significant added values in metallic alloys is the main interest in this field. The LBM process involves a focused laser beam which selectively melts a thin bed of spread powder material. This step is repeated track-by-track and layer-by-layer until the final product is obtained. During the laser scan, fast melting and solidification phenomena occur. The cooling rate has a major impact on the microstructure and mechanical properties of the final part [1, 2]. As a consequence, it is required to have an accurate estimation of these terms in order to determine the final state of the pieces. Numerical simulation represents a useful tool to predict the occurence of defects, such as porosities or cracks, regarding the cost to determine optimal operating parameters.

A numerical Finite Element (FE) 3D model for LBM process adapted for metals is presented [3]. This model is focused on the thermomechanical evolution of material at the scale of the bead. The laser-matter interaction is modeled by two different terms. A volume Beer-Lambert source for the laser-powder interaction and a surface source for the laser-dense material interaction. During the development of the melt pool, capillary and boiling effects occur, having influence on the melt pool shape [4]. In addition, the model considers an automatic remeshing procedure which avoids huge CPU cost due to mesh constraints [3].

2. Modeling

This FE model is based on the work of Chen at CEMEF [3]. The system is made of a material and a gas domain. The main assumptions of the model are as follows :

- The powder bed is considered as a continuum domain with a given porosity ;
- The densification of the powder bed is a one-way transformation.

During the heating stage, the powder bed melts continually to form a compact deposition. This transformation occurs by the evolution of the apparent density of the material powder, depending of the temperature, also considering a transition domain.

2.1. Level-set Method

The total system is made of a material D_1 and a gas domain D_2 (Figure 1). A signed distance function ψ is used respecting the eikonal condition $|| \nabla\psi || = 1$. The evolution of the position of the interface is tracked by the resolution of the transport equation of this distance function [5] :

$$\frac{\partial\psi}{\partial t} + \mathbf{u} \cdot \nabla\psi = 0 \tag{1}$$

where $\mathbf{u}$ is the velocity field induced by the powder shrinkage and the melt pool evolution defined on the whole domain. A geometric reinitialisation method is used in order to respect the eikonal condition after the transport step [6]. The local average properties are computed with the Heaviside function corresponding to the transition domain [5].

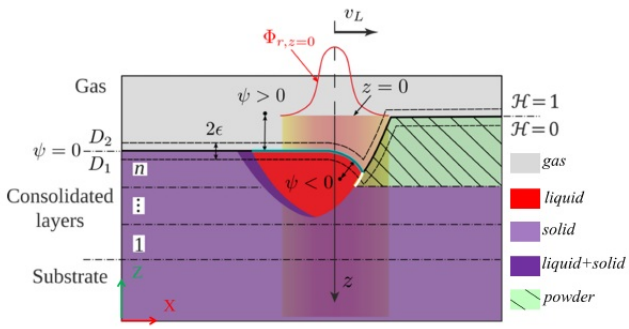

Figure 1. Schematic of the LBM process with the level-set (LS) method to track the interface associated to the isovalue $\psi = 0$ of the signed distance function [3].

2.2. Governing equations

2.2.1. Energy conservation and heat source modeling

The computation of the temperature field is required to propose accurate prediction of the different phenomena that occur during the LBM process. We may consider the influence of this field on phase transformations, the development of a recoil pressure or Marangoni forces. These different phenomena affect the shape of the bead. Considering the fast thermal evolutions observed in AM processes, it is necessary to take into account the temperature variation of physical properties. The modeling of the heat transfer in LBM is obtained as the solution of the non-steady equation of energy conservation :

$$\frac{\partial \{\rho h\}}{\partial t} + \nabla \cdot (\{\rho h\} \mathbf{u}) - \nabla \cdot (\{\lambda\} \nabla T) = \dot{q}_L \tag{2}$$

$$\{\rho h\} = f(T) \tag{3}$$

where ρ is the density, h the specific enthalpy, λ the thermal conductivity and T the temperature. $\dot{q}_L$ represents the heat source associated to the laser.

The laser interacts mainly with the powder bed and the melt pool. The laser follows a radial Gaussian distribution also considering a reflection coefficient R. Consequently, the heat source can be shared as two terms depending on the state of the surface :

$$\dot{q}_L = \begin{cases} (1-R)\frac{2P_L}{\pi r_{int}^2} e^{-\frac{2r^2}{r_{int}^2}} \left(\alpha e^{-\int_0^z \alpha dl}\right) & \text{[Laser - Powder bed interaction] [3]} \\ (1-R)\frac{2P_L}{\pi r_L^2} e^{\frac{-2r^2}{r_L^2}} \cdot \delta_2(\psi) & \text{[Laser - Dense material interaction] [7]} \end{cases} \tag{4}$$

Where P_L is the laser power, r_{int} the interaction radius, r_L the laser radius and α the local value of absorption coefficient. A volumetric Beer-Lambert law has been chosen to take into account the multiple reflections taking place in the powder bed and the progressive absorption of laser radiation in the material. It is assumed that the laser energy is totally absorbed after four reflections ($R^{n_r} \cdot (1-R) < 0.07$, $\forall n_r > 4$ where n_r is the number of reflections) [8]. For the laser - dense material interaction (liquid and solid phase), the surface heat source model is more representative regarding the high absorption of laser energy by dense metallic material.

2.2.2. Momentum conservation
The convective flow has a major influence on the temperature field and the melt pool shape. Consequently, the fluid flow evolutions in the liquid domain are limited to the dimension of the melt pool. Fluid dynamics equations are established by the mass and momentum conservation equations (Navier-Stokes). To take into account the change of apparent density in the powder bed during the melt stage, compressible flow has to be considered in the moment conservation equation :

$$\nabla \cdot \mathbf{u} = \dot{\theta} = -\frac{1}{\{\rho\}} \cdot \frac{\partial \{\rho\}}{\partial t} \tag{5}$$

$$\{\rho\} \left(\frac{\partial \mathbf{u}}{\partial t} + (\mathbf{u} \cdot \nabla)\mathbf{u} \right) - \nabla \cdot \bar{\bar{\boldsymbol{\sigma}}} = \mathbf{f_v} \text{ where } \bar{\bar{\boldsymbol{\sigma}}} = 2\mu \left(\bar{\bar{\boldsymbol{\epsilon}}} - \frac{1}{3} tr(\bar{\bar{\boldsymbol{\epsilon}}}) \bar{\bar{\mathbf{I}}} \right) - p\bar{\bar{\mathbf{I}}} \tag{6}$$

where $\dot{\theta}$ is the variation rate due to the shrinkage of the powder to dense matter, $\bar{\bar{\boldsymbol{\sigma}}}$ is the stress tensor, μ is the dynamic viscosity and $\mathbf{f_v}$ are the volumetric forces. These forces contribute to the dynamic of the melt pool and have several origins. Firstly, capillary effects represented by the surface tension and the Marangoni forces have to be considered. The recoil pressure during the vaporisation phase is also considered and induces the deflection of the interface by the high velocity vapour metal that is ejected. In addition, buyoancy forces are introduced. The whole forces are then written as :

$$\mathbf{f_v} = \mathbf{f_v^{STn}} + \mathbf{f_v^{STt}} + \mathbf{f_v^{recoil}} + \mathbf{f_v^{g}} \tag{7}$$

where :

- $\mathbf{f_v^{STn}} = \gamma\kappa\delta\mathbf{n}$ represents the surface tension force [3].
- $\mathbf{f_v^{STt}} = \delta\frac{\partial\gamma}{\partial T}\nabla_s T$ is the Marangoni force induces by the temperature dependence of the surface tension force. This dependency induces a shear stress at the liquid/gas interface in an parallel direction to the temperature gradient [3].
- $\mathbf{f_v^{recoil}}$ is the force generated by the intense ejection of metallic vapour [9].
- $\mathbf{f_v^{g}} = \{\rho\}\,\mathbf{g}$ are the buoyancy forces due to local variations of density with temperature.

3. Numerical tests
Different configurations are presented using material data for Inconel 718 alloy. The first cases correspond to static laser shooting and the second case to track development.

3.1. Static laser shooting on solid substrate
Static shooting on a substrate and secondly on a powder bed (LBM) are considered. The different parameters (machine and properties of Inconel 718) are detailed in Figure A1. The expression of the recoil pressure has been also simplified for this study with a surface force independent of temperature and following a radial Gaussian distribution :

$$\mathbf{f_v^{recoil}} = -\left(\frac{1+\beta_r}{2} \right) \cdot 1.63 \cdot p_0 \cdot e^{\frac{-2r^2}{r_L^2}} \delta(\psi)\mathbf{n} \tag{8}$$

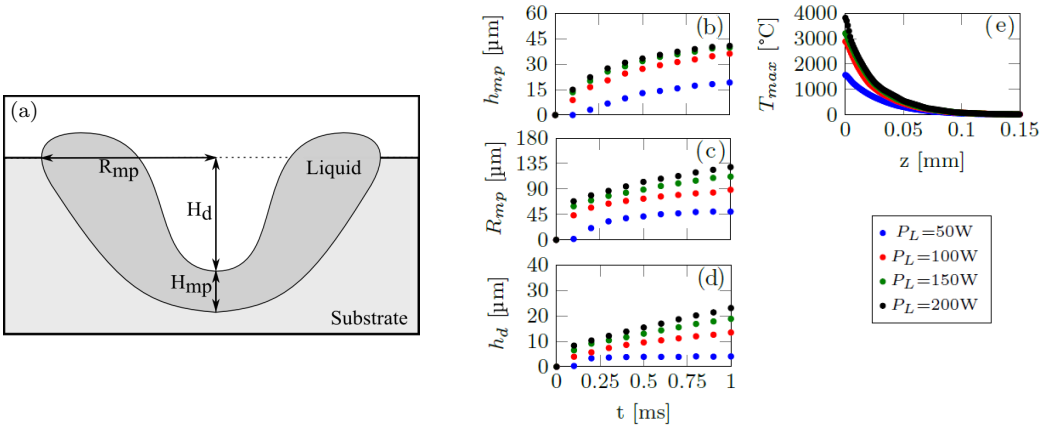

Figure 2. (a) Definition of liquid dimensions. (b), (c) and (d) are respectively the evolution of the melt pool height h_{mp}, the melt pool radius at the surface R_{mp} and the deflection of the interface h_d due to recoil pressure force. (e) Evolution of the maximal of temperature field observed in the material with depth.

where $\beta_r = 0.17$ is the retrodiffusion coefficient. The different simulations are compared in Figure 2 when considering various laser power. The vaporisation still does not occur in the material for a laser power of 50 W after 1 ms of laser shooting. Slight variations in the evolutions of the melt pool height h_{mp} and the radius of the melt pool R_{mp} are observed after 1 ms of laser shooting. A balance is observed between the heat introduced by the laser and the one extracted through the substrate by thermal conduction. As the convection in the melt pool is dominant regarding the other phenomena, the maximum of temperature reached after 1 ms of laser shooting increases more and more slowly when the laser power increases.

3.2. Static laser shooting on a powder bed

The second case investigated is a static shoot on a powder bed with a thickness h_p and a porosity of 50 %. The laser power is equal to 250 W with a radius of 50 µm. the different properties of the material are detailed in the Appendix (Figure A1). The different stages

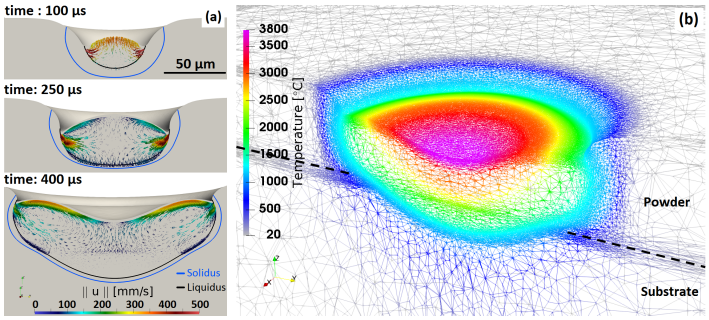

Figure 3. (a) Stages obtained during the SLM process in the case of a laser shooting. (b) Evolution of the temperature field and the anisotropic mesh at t=400 µs.

during the SLM process are predicted by the model as shown on Figure 3.(a) : the beginning of the compaction of the powder bed into a melt pool, the spheroidization of the melt pool occurs due to the surface tension and finally, the deflection of the interface when the vaporisation stage is reached due to the recoil pressure. On the Figure 3.(b), the maximum of temperature observed is approximatly 3800°C. This temperature is much greater than the vaporisation temperature chosen in the model. The maximum in velocity magnitude observed in this simulation is close to 500 mm/s.

3.3. Single pass on a powder bed

The configuration investigated is similar to the first case except that the domain is larger (1500 mm × 1000 mm × 1100 mm) with a continuous displacement of the laser. The different properties in the Appendix are used for this numerical simulation. The different results are shown in Figure 4. The development of a single bead is computed. For this

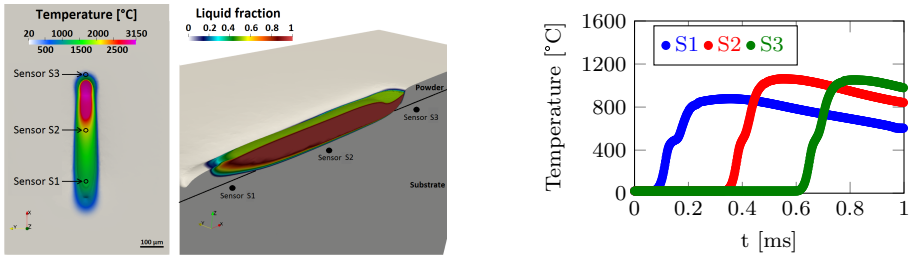

Figure 4. Temperature field and liquid fraction g_l at t=0.65 ms (left) and evolution of the temperature with time measured on three virtual sensors S1, S2 and S3 (right).

configuration, the powder is completly melted whereas the substrate is barely melted. The different virtual sensors shown in Figure 4 are located 10 µm below the surface of the substrate to observe if melting occurs. The temperature reached at this depth is 200°C below the liquidus. The bead obtained is not acceptable regarding SLM processes since it is crucial to merge the bead with the substrate. The input linear energy is not high enough to melt the substrate more deeply. Nevertheless, it should be relevant to get experimental results since it is possible that the reflection coefficient is overestimated or the material properties are not fully realistic.

4. Conclusion

A level-set model of SLM process applied to metals is presented to follow track evolution. The laser-matter interaction is described by a volume heat source between the laser and the powder bed and a surface source between the laser and the dense matter. Surface tension, Marangoni forces and the recoil pressure at the vaporisation stage are considered in order to provide an accurate modelling of the melt pool development.

Two configurations are investigated in this context. The first case corresponds to a laser shooting on a substrate and on a powder bed and the second case to a single track simulation on a powder bed. These configurations will be compared at a laser stage with the results provided by the commercial software Comsol Multiphysics® and experiments in a context of a benchmark with Arts et Métiers ParisTech.

The next step is to compute several unidirectional single passes to understand the influence of previous solidified tracks on the surface morphology. Finally, an interesting perspective is to simulate the build of a wall to observe the influence of the previous powder bed layer on the results obtained for the following one and compare these results with experimental data observations on surface stage of pieces and interaction between passes.

References

[1] Z. Wang, K. Guan, M. Gao, X. Li, X. Chen and X. Zeng. *Journal of Alloys and Compounds*, 513 :518–523, 2012.
[2] T. Antonsson and H. Fredriksson. *Metallurgical and Materials Transactions B*, 36(1) :85–96, 2005.
[3] Q. Chen, G. Guillemot, CA. Gandin and M. Bellet. *Additive Manufacturing*, 16 :124–137, 2017.
[4] F. Verhaeghe, T. Craeghs, J. Heulens and L. Pandelaers. *Acta Materialia*, 57(20) :6006–6012, 2009.
[5] M. Sussman, P. Smereka and S. Osher. *Journal of Computational physics*, 114(1) :146–159, 1994.
[6] M. Shakoor, B. Scholtes, P-O. Bouchard and M. Bernacki. *Applied Mathematical Modelling*, 39(23) :7291–7302, 2015.
[7] V. Bruyere, C. Touvrey, P. Namy and N. Authier. *Journal of Laser Applications*, 29(2) :022403, 2017.
[8] X. Jin, L. Li and Y. Zhang. *Journal of Physics D : Applied Physics*, 35(18) :2304, 2002.
[9] S. Anisimov and V. Khokhlov. CRC press, 1995.
[10] Web site. Dry air properties. `https://www.engineeringtoolbox.com/dry-air-properties-d_973.html`.
[11] C. Mills, C. Kenneth. Woodhead Publishing, 2002.
[12] P. Zehner and E.U. Schlünder. *Chemie Ingenieur Technik*, 42(14) :933–941, 1970.

Appendix :

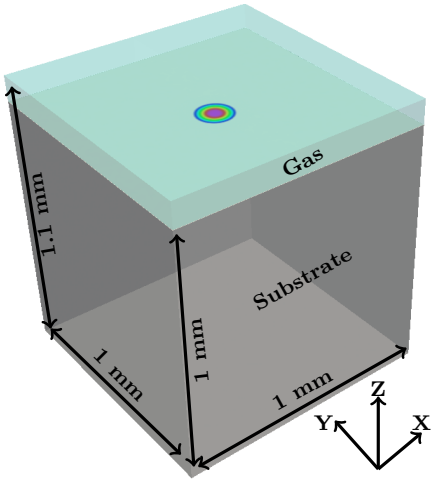

Welding	Property	Symbol	Value	Unity
Laser	Power	P_L	[50−200]	W
	Radius	r_L	75	µm

LBM	Property	Symbol	Value	Unity
Laser	Power	P_L	250	W
	Radius	r_{int}	50	µm
	Speed	v_L	1.1	$\mathrm{m\,s^{-1}}$
Powder Bed	Thickness	h_p	50	µm
	Porosity	ϕ_p	0.5	–
	Absorption	h_p	20	$\mathrm{mm^{-1}}$
	Thermal conductivity	λ_p^{ZS}	Fig 5(b)	$\mathrm{W\,m^{-1}\,K^{-1}}$
	Viscosity Dynamic	μ_p	Fig 5(c)	Pa s

Material	Property	Symbol	Value	Unity	Ref.
Argon	Density	ρ_g	1.78	$\mathrm{kg\,m^{-3}}$	
	Thermal conductivity	λ_g	0.024	$\mathrm{W\,m^{-1}\,K^{-1}}$	[10]
	Enthalpy per unit mass	$C_{p,g}$	Fig 5	$\mathrm{J\,kg^{-1}\,K^{-1}}$	
	Absorption coefficient	α_g	0	$\mathrm{m^{-1}}$	[–]
IN718	Solidus	T_s	1443	K	
	Liquidus	T_l	1609	K	
	Boiling	T_v	3184	K	
	Absorption (liquid)	α_l	120	$\mathrm{mm^{-1}}$	
	Density solid, liquid	ρ_s, ρ_l	8190, 7300	$\mathrm{kg\,m^{-3}}$	
	Thermal conductivity	λ	26.9	$\mathrm{W\,m^{-1}\,K^{-1}}$	[11, 12]
	Enthalpy per unit mass	h_m	Fig 5(a)	$\mathrm{J\,kg^{-1}\,K^{-1}}$	
	Latent heat of fusion	L_f	270	$\mathrm{kJ\,kg^{-1}}$	
	Latent heat of vaporisation	L_v	6690	$\mathrm{kJ\,kg^{-1}}$	
	Surface tension	γ	1.89	$\mathrm{N\,m^{-1}}$	
	Marangoni coefficient	$\frac{\partial\gamma}{\partial T}$	$-1.1\cdot10^{-4}$	$\mathrm{N\,m^{-1}\,K^{-1}}$	
	Dynamic viscosity (liquid)	μ_d (μ_l)	Fig 5(c) ($7.8.10^{-3}$)	Pa.s	

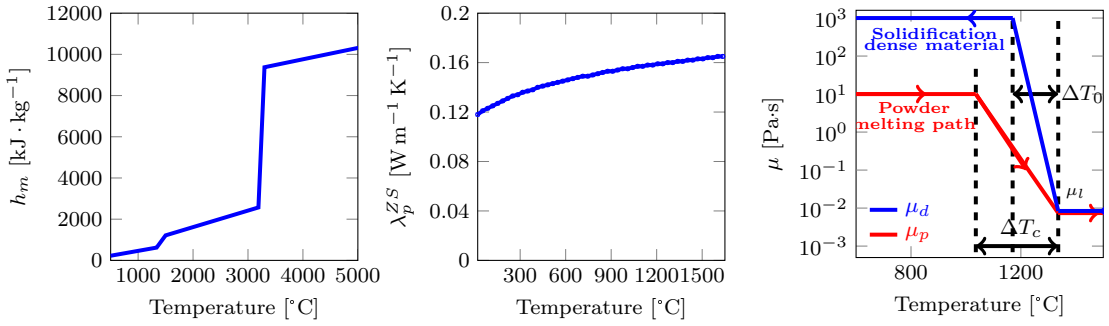

(a) (b) (c)

Figure A1. Configuration studied (domain and machine) for a welding or SLM simulation, properties chosen for Inconel 718 alloy and evolution of the specific enthalpy h_m, thermal conductivity in the powder λ_p^{ZS} and the dynamic viscosity μ with temperature. ΔT_0 and ΔT_C are respectively the temperature range of the melting stage and compaction (larger than the melting stage one to avoid numerical convergence issues) of the powder bed in a melt pool [3].